Identification and quantification of within-burst dynamics in singly labeled single-molecule fluorescence lifetime experiments

Paul David Harris[1,*], **Eitan Lerner**[1,2,*]

[1]Department of Biological Chemistry, The Alexander Silberman Institute of Life Sciences, Faculty of Mathematics & Science, The Edmond J. Safra Campus, The Hebrew University of Jerusalem, Jerusalem 9190401, Israel

[2]The Center for Nanoscience and Nanotechnology, The Hebrew University of Jerusalem, Jerusalem 9190401, Israel

Abstract

Single-molecule spectroscopy has revolutionized molecular biophysics and provided means to probe how structural moieties within biomolecules spatially reorganize at different timescales. There are several single-molecule methodologies that probe local structural dynamics in the vicinity of a single dye-labeled residue, which rely on fluorescence lifetimes as readout. Nevertheless, an analytical framework to quantify dynamics in such single-molecule single dye fluorescence bursts, at timescales of microseconds to milliseconds, has not yet been demonstrated. Here, we suggest an analytical framework for identifying and quantifying within-burst lifetime-based dynamics, such as conformational dynamics recorded in single-molecule photo-isomerization-related fluorescence enhancement. After testing the capabilities of the analysis on simulations, we proceed to exhibit within-burst millisecond local structural dynamics in the unbound a-synuclein monomer. The analytical framework provided in this work paves the way for extracting a full picture of the energy landscape for the coordinate probed by fluorescence lifetime-based single-molecule measurements.

INTRODUCTION

The advent of single-molecule fluorescence spectroscopy (SMFS) has been a boon to structural biology, allowing conformations to be directly observed, rather than the ensemble average of a large group of molecules with multiple unsynchronized conformations (1,2). There are a variety of SMFS modalities, which vary in time resolution (2), and all rely on attaching fluorophores to a biomolecule, such as a protein or nucleic acid under study. These

*Correspondence: paul.harris@mail.huji.ac.il or Eitan.Lerner@mail.huji.ac.il.

methods vary both by whether a confocal or wide-field microscope is used and by what fluorescence phenomenon is exploited, such as Förster resonance energy transfer (FRET), photo-induced electron transfer (PET) (3,4), or photo-isomerization-related fluorescence enhancement (PIFE; commonly known as protein-induced fluorescence enhancement) (5–10).

Confocal-based methods provide the highest time resolution, using detectors sensitive to the arrival of individual photons, and typically record interphoton times on the order of a few microseconds (11, 12). In these experiments, single molecules traverse the confocal volume, and while doing so undergo multiple excitation-emission cycles. This results in periods of high photon count rate, referred to as photon bursts, which typically last a few milliseconds. In traditional burst analysis, the photon detection events of each burst are aggregated to form a single data point per burst. This is ideal for biomolecules that undergo dynamic transitions at timescales slower than milliseconds, termed "between-burst dynamics." However, when dynamic transitions occur in timescales on the order of burst durations or faster, termed "within-burst dynamics," molecular sub-populations blur together and require alternative techniques that analyze the photon stream(s) directly to uncover the dynamics hidden in the blurred burst parameter histograms.

Methods such as probability distribution analysis (PDA) (13), burst variance analysis (BVA) (14,15), and others (2) exist to quantify within-burst dynamics in confocal-based single-molecule FRET experiments. These methods rely on the fundamentally centrally distributed ratiometric parameter of the FRET efficiency. It is common in other modalities, however, to rely on the fundamentally exponentially distributed parameter of fluorescence lifetime. These specific modalities, however, might lack equivalent ways of quantifying within-burst dynamics in confocal-based single dye fluorescence lifetime experiments. In that respect, fluorescence correlation spectroscopy is sensitive to correlations in fluorescence intensity occurring at different timescales for different types of fluorescence dynamic processes, and as such can, in principle, detect these single dye fluorescence dynamics processes (16). Two-dimensional (2D) fluorescence lifetime correlation spectroscopy (2D-FLCS) (17,18) is capable of detecting fluorescence lifetime dynamics in single dye fluorescence measurements, but requires a large dataset and could suffer from numerical instabilities (see section "discussion"). Thus, methods to efficiently and accurately quantify within-burst dynamics in confocal-based single dye fluorescence lifetime experiments are required.

Out of several modalities that introduce excited-state fluorescence modulation (i.e., either quenching or enhancement), PIFE is of particular interest because 1) it only requires a single dye, simplifying labeling procedures and minimizing the potential structural perturbation that dye labeling may introduce to the biomolecule under study; and 2) the fluorescence quantum yield, and therefore the molecular brightness, and the fluorescence lifetime of the dye have been shown to be monotonically related to the proximity of the dye to the biomolecular surface in the 0–3 nm range (5,6,8,19,20), among other potential reasons that affect the dye fluorescence lifetime.

The dye-protein proximity dependence in PIFE renders it not only an attractive method on its own but also a nice complement to FRET (8), having sensitivity to distances smaller than the scale of distance sensitivities in FRET.

Using this effect, we were able to observe different groupings of photon bursts of freely diffusing sulfo-Cy3 (sCy3)-labeled biomolecules based on the mean value of all photon nanotimes (i.e., mean nanotime), the photon detection times relative to the moments of excitation that led to these photon emission events (sometimes referred to as photon microtimes). Bursts with short mean nanotimes are associated with a biomolecular structure having minimal steric hindrance on the sCy3-labeled residue, while those with longer mean nanotimes are associated with a biomolecular structure having a relatively restricted steric environment in its vicinity. This assessment, however, still relied on assessing single-molecule bursts over a time-integrated parameter, and therefore the possibility of within-burst dynamics could not be precluded, and no method has been introduced for the analysis of within-burst dynamics in single-molecule PIFE (smPIFE) experiments.

Therefore, we aspired to develop a method to quantify within-burst dynamics in single dye single-molecule fluorescence lifetime-based measurements such as smPIFE. For this, we sought to adapt the multi-parameter photon-by-photon hidden Markov modeling (mpH^{2}MM) framework (21,22) that we recently introduced to function with photon nanotime data, which has previously only been applied to FRET-based applications. We therefore introduce a simple and widely implementable scheme to transform the exponential distribution of photon nanotimes into set of tractable parameters, amenable for use with mpH^{2}MM.

In this work, we first use simulations to assess the applicability and limitations of our scheme to find within-burst dynamics using photon nanotimes. We then apply it to smPIFE data of freely-diffusing unbound α-synuclein monomer, and are able to quantify the transition rates between two conformational sub-populations.

RESULTS

The divisor approach

Single photon counting data can include the absolute photon detection time, relative to the moment data acquisition started (the photon macrotime), and also the delay between the moment of excitation and photon detection for each detected photon (the photon nanotime, also referred to as the photon microtime; in the rest of this text, we will exclusively use the term nanotime to prevent confusion). The maximal photon nanotime value corresponds to the reciprocal of the laser repetition rate, creating a range of potential photon nanotime values. In time-correlated single photon counting (TCSPC) systems, the photon nanotime can be measured with picosecond precision, hence each TCSPC time bin can report on photon nanotimes with uncertainties in the picosecond timescale. When a large number of photons have been detected, the histogram of the photon nanotimes can be used for representing the fluorescence decay (Fig. 1 d). Unfortunately, a single burst typically contains far too few photons to construct a smooth fluorescence decay that is useful in decay fitting. Therefore, alternative methods, such as maximum likelihood estimation (MLE) (23),

or the phasor approach (24), are used for determining the fluorescence lifetime from smaller number of photons. Even these methods, however, have no way to distinguish a transition between 1) distinct single fluorescence lifetime states occurring within a single-molecule photon burst, hence within-burst dynamics; and 2) a single-molecule photon burst reporting on dwell in a single state characterized by a multi-exponential decay.

A powerful method for identifying within-burst dynamics is photon-by-photon hidden Markov modeling (H^{2}MM), introduced by Pirchi et al. (21), of which we have made extensive use, recently leading to the multi-parameter version of H^{2}MM (mpH^{2}MM) (22). In H^{2}MM, the basic framework of hidden Markov modeling (HMM) is extended to accept the variable interphoton times. Each photon forms a datapoint, with a pair of values: the detection time (i.e., photon macrotime) and some measured parameter, such as on which detector was the photon detected. This measured parameter must have an integer value. Each state has a distinct probability of producing each of the possible parameter values, which are recorded in the emission probability matrix.

In our previous work, the parameters were the detection channels and excitation sources within alternating laser excitation (25–27) (ALEX; or pulsed interleaved excitation (PIE) (28)) setups, but the underlying algorithm is not limited to this type of parameterization. The typical TCSPC acquisition card records photon nanotimes in a predefined number of time bins, thus photon nanotimes have an integer set of values. Hence photon nanotimes can be used as input for mpH^{2}MM. However, the typical number of TCSPC time bins is 4,096 per excitation cycle, leading to the low probability of a photon arriving in a given time bin. This, in turn, leads to poor, and oftentimes slower, optimizations, especially in applications with low photon counts, rendering the use of raw photon nanotime bins a poor choice for using mpH^{2}MM. To reduce the number of possible parameter values for mpH^{2}MM, we introduce a divisor approach. A divisor is simply a threshold of TCSPC time bins, where TCSPC time bins between two divisors are all treated as having the same parameter value (Fig. 1). As an example, with a single divisor, there are two possible parameter values, before and after the divisor. With two divisors (as shown in Fig. 1), there are three possible values, before both, between, and after both; with three divisors, the pattern continues with there being four possible parameter values, and so on. There is a trade-off where, with more divisors, the resolvability increases, which increases the likelihood of detecting smaller changes in fluorescence lifetime, but the probability of a given photon having a given parameter value decreases as well, which tends to increase the probability of a failed or improper optimization. Therefore, we seek to find the optimal balance in assignment of these divisors.

We note that, in the case of a single divisor, the proposed approach reproduces Kim et al.'s promptness ratio. Adapting Eq. 2 from Kim et al.'s work, we can derive an expression for the fluorescence lifetime of a state characterized by a mono-exponential decay, as shown here in Eq. 1:

$$\tau = \frac{T}{\ln(p_0)}. \tag{1}$$

where τ is the fluorescence lifetime, T is the time between the laser pulse time and the divisor, and p_0 is the fraction of photons detected with photon nanotimes smaller than the divisor value. Importantly, Kim et al. noted that the sensitivity to different fluorescence lifetime values and to multi-exponential decays depends on the choice of the single divisor value, therefore the same can be expected in our analysis. Such greater sensitivity can be achieved using multiple divisors. Therefore, to determine the ideal balance, we tested a total of eight divisor schemes, where a scheme is a method of choosing divisors, with different numbers of divisors and methods for determining their positions (see section "experimental methods").

Simulations

Using PyBroMo (29,30), we simulate fluorescently-labeled single dye diffusing biomolecules transitioning between two fluorescent states with two distinct fluorescence lifetimes at varying rates from as slow as $10\ \mathrm{s}^{-1}$ to as rapid as $10,000\ \mathrm{s}^{-1}$. The fluorescence quantum yield value of each state scales linearly with the fluorescence lifetime of each state (see section "appendix"). Therefore, these conditions simulate single dye fluorescence lifetime-based experiments with fluorescence modulation solely due to excited-state modulation (e.g., excited-state quenching or enhancement), and hence without ground-state modulations (e.g., ground-state quenching). The short fluorescence lifetime of the first state is either 1.2 or 1.6 ns, and the long florescence lifetime of the second state is either 3.2 or 3.6 ns, with all combinations of short and long lifetimes simulated. The simulated single-molecule burst data are analyzed using FRETBursts (31) to identify single-molecule bursts. For simulations where both transition rates are slow compared with burst duration (<100 s^{-1}), different mean nanotime sub-populations are clearly distinguishable for each state. For faster transition rates, more bursts of intermediate mean nanotime values are present, forming a bridge between the short and long lifetime sub-populations (Fig. 2 a). This blurring of sub-populations results from transitions between states of different fluorescence lifetimes and quantum yields, while the dye-labeled biomolecule traverses the effective excitation volume. There is a bias in burst selection for bursts of the longer fluorescence lifetime state. This is due to the higher fluorescence quantum yield of the long lifetime sub-population, resulting in higher photon rates, which are more likely to have photon count rates above the signal-to-background threshold used for identifying bursts. Thus, in single dye fluorescence lifetime-based applications, where the fluorescence lifetime is linearly proportional to the fluorescence quantum yield (e.g., smPIFE, excited-state quenching; see section "appendix"), an inherent bias will occur in burst selection for longer lifetime bursts.

Before quantitatively analyzing the data using the mpH^{2}MM approach, we tested photon statistics methods that assisted in indicating the presence or absence of within-burst dynamics in FRET, such as BVA (14) and two-channel kernel-based density distribution estimator (2CDE) (32), but adapted to identifying within-burst transition dynamics in fluorescence lifetime data. Our tests have shown that these approaches are not useful for analyzing within-burst dynamics in single dye SMFS data (see detailed discussion in the Supporting Material and Figs. S1 and S2).

Then, we perform mpH^{2}MM analyses of all burst photon data, using our divisors schemes, and we compare the results of the mpH^{2}MM analyses of the simulated data with the known ground-truth parameter values. The main purpose of mpH^{2}MM here, and in general, is to identify underlying states. Since the number of underlying states is usually unknown prior to analysis, and since mpH^{2}MM is able to optimize models with any number of states, multiple optimizations must be conducted with different state models. After this, the model that best represents the data will be identified. Therefore, a statistical discriminator is necessary for identifying the ideal model. Similar to FRET-based applications, we find that the integrated complete likelihood (ICL) (22) is a good statistical discriminator. Models with more states than necessary are considered over-fit, where the model contains non-existent states, or splits what should be a single state into multiple ones based on what is actually statistical noise in the data. On the other hand, models with fewer states than necessary are under-fit, missing certain states entirely or treating two states as one. We find that the ICL selects the correct number of states in most cases (Figs. 2 b, c, and S3–S6). The two key limitations are that the number of consecutive photons in a given state must be sufficient (Figs. 2 b and S4–S6), and that there must be a sufficient number of instances of a given state for it to be detectable. When these limitations came into play, the ICL was usually minimized for the single state case (Figs. 2 c and S4–S6). The ICL was rarely minimized for three-state models, indicating that the ICL rarely selects an over-fit model (Table S1). These over-fit models all show features of over-fitting that make it a simple task for the user to screen for such models (Fig. S7).

To assess the influence of the size of the dataset, we also analyzed truncated versions of our simulated data. In most cases, the ICL remained minimized at nearly identical results (Figs. S8–S11).

Then we assess the accuracy of the Viterbi algorithm, which finds the most-likely state of each photon given the optimized model and the recorded photon data. Since the simulation records the state of the molecule for each photon detection time, we could compare this state with that determined by the Viterbi algorithm. We found that the Viterbi algorithm was ~95% accurate in assigning the correct photons to their underlying states (Fig. 2 d and e). For states represented by fluorescence decays with a single fluorescence lifetime component, all divisor schemes we tested have nearly identical accuracy. However, divisor schemes with more divisors were more likely to select the two-state model based on ICL, while the ICL of divisor schemes with fewer divisors were more likely to select under-fit single-state models. Since, in many cases, practical systems will involve multi-component decays, it is therefore advisable to rely on divisor schemes with multiple divisors (see Table S1).

Comparing ground-truth transition rates with those detected by mpH^{2}MM, we note a degree of deviation. The recovered transition rates from the short fluorescence lifetime state are consistently faster than the ground-truth values, while the recovered transition rates from the long fluorescence lifetime states are consistently slower (Figs. 3 a and b, S12–S14, repeats of this figure for other lifetime combinations, and Fig. S15 for more detailed summary). This deviation is likely due to there being proportionally more photons emitted from the long lifetime state per unit time compared with the short fluorescence lifetime state, biasing the results toward the long fluorescence lifetime state. In all cases, the deviation was still

a factor of at most three compared to ground-truth transition rates that can be considered comparable, and thus mpH^{2}MM extracts reasonable dynamics so long as transition rates are within an order of magnitude of the burst duration.

Finally, we turn to assessing the accuracy of fluorescence lifetimes in states assessed by mpH^{2}MM. This can be assessed in multiple ways. If a single divisor is used, it can be treated using Eq. 1. However, for multi-divisor schemes, multiple potential lifetimes can be calculated, and thus deriving the fluorescence lifetime is non-trivial. We therefore prefer to use the results of the Viterbi algorithm to assign photons to states, build fluorescence decays, and extract the fluorescence lifetime values from these decays. Further confirming the accuracy of Viterbi/mpH^{2}MM, these decays are consistent with the ground-truth fluorescence lifetimes. The extracted fluorescence decays closely mirror the ground-truth (Figs. 3 b, c, and S12–S14). Fitting these fluorescence decays to exponential decays, we retrieve fluorescence lifetimes that are within 0.2 ns of the ground-truth (Fig. 3 e and f). When we use multi-exponential decays, specific lifetime components were less precise with fittings; however, the correspondence of the decays with the available ground-truth photons indicates that our inaccuracies were more a result of the lack of photons in each lifetime component, due to the short time of our simulations, and, given larger datasets, similarly accurate fluorescence lifetimes could likely be extracted.

Individual dwells in a state lack sufficient photons to construct fluorescent decays, but the mean photon nanotimes in dwells can still be used. Whether dealing with bursts or dwells within bursts, the mean of the distribution is slightly larger than the simulated ground-truth lifetime values. We found that this is the result of two primary factors: 1) background photons, which are equally probable at any point in the fluorescence decay; and 2) the exclusion of the instrument response function (IRF). When background photons are excluded, mean photon nanotimes decrease, but still exhibit larger values than the ground-truth values of the simulation (Fig. 3 e).

Regarding the shape of the acquired mean nanotime histograms, while histograms of burst-based mean photon nanotimes have variable shapes, indicative of multiple sub-populations, once we use mpH^{2}MM and the Viterbi algorithm to segment the data into dwells in states, the dwell-based mean photon nanotimes of each state generally follow a central distribution. Naively, following the central limit theorem (CLT), the histogram of mean photon nanotimes in a state would be expected to follow a normal distribution. However, as photon nanotimes cannot have negative values, especially for short fluorescence lifetime states, the distribution cannot strictly be described by Gaussians. Additionally, since the CLT is true for a sufficient amount of photon nanotimes sampled from a given distribution, and since time dwells in a state sometimes include many photon nanotimes but in other times just a few, we expect to get mean photon nanotime histograms per state that deviate from a Gaussian distribution also due to instances with means of lower amount of photons. Nevertheless, we still report the mean nanotime histograms in dwells per state, and they are clearly centrally distributed with varying widths, but we do not impose the use of Gaussians in fitting due to the above explanations.

Overall, our simulations demonstrate that mpH^{2}MM is capable of disentangling within-burst dynamics in single dye fluorescence lifetime data. While some systematic bias favors states with higher intrinsic brightness, the fundamental recovery of both fluorescence lifetime states and the transition rate data is sound.

smPIFE-based millisecond transitions in unbound a-synuclein monomer

After testing the applicability of the multi-divisor approach and mpH^{2}MM on simulations, we demonstrate the usefulness of this approach on an important biomolecular system. a-Synuclein (a-syn) is an intrinsically disordered protein that self-associates into oligomers, aggregates, and amyloid fibrils, and is implicated in the molecular etiology of Parkinson's disease, among other neurodegenerative diseases (33–35). Upon binding to membranes or self-associating, a-syn can gain partial folded structures (36–43). However, when unbound, a-syn is mostly unstructured (44) and exhibits conformational dynamics with relaxation times in the hundreds of nanoseconds, as has been shown before in the analyses of single-molecule FRET measurements (38,45). These important findings were focused on the dynamics of the distance between pairs of dye-labeled residues far apart in the main polypeptide chain, and using the 3–10 nm distance sensitivity that single-molecule FRET provides (2). These results report on the dynamic nature of the disordered unbound a-syn within the 3–10 nm distance scale typically characterizing nonlocal interactions in small proteins.

Interestingly, we have recently used smPIFE, among other methods, to investigate the conformational dynamics of the unbound a-syn monomer (46). Histograms of burst-based mean nanotimes indicated that there are at least two interconverting a-syn sub-populations, each with distinct mean photon nanotime values. These results indicate that structures in the <3-nm distance sensitivity of PIFE, typically considered local for proteins, persist for longer times than the FRET measurements have shown for nonlocal interactions. Fluorophore-protein stacking interactions and other interactions that are irrelevant to protein structural changes typically exhibit sub-microsecond relaxation times (47,48). Thus, it is unlikely that these results are due to an interaction of the protein and the sCy3 dye, which are not related to actual structural changes. However, we note that such a possibility cannot be categorically ruled out. Following this, burst recurrence analysis of single particles (RASP) (49) indicated a signature of transition dynamics between these sub-populations in the millisecond timescale. RASP, however, reports on between-burst dynamics, which represents timescales longer than the ones that may occur within bursts. We therefore applied our divisor approach with mpH^{2}MM to this data to see if within-burst dynamics could be detected, and perhaps the transition rates quantified.

We test this on the unbound a-syn monomer singly labeled with sCy3 at residues 26, 56, and 140. Across multiple divisor schemes that we tested, the ICL predicts two states. While two states are consistently identified, the transition rates for different labeling residues vary. At residue 26, the transition rates are <100 s^{-1}, with almost no within-burst transitions found. At residues 56 and 140, however, the transition rates were larger than that value (<330 s^{-1}), indicating a degree of within-burst dynamics. The difference in the transition rates for the different labeled residues could indicate slightly different dynamics, but all on

a timescale within the same order of magnitude of a few milliseconds. Using the Viterbi algorithm to segment the data into dwells in states, we generate histograms of the mean fluorescence lifetimes of dwells, enabling the recovery of state-relevant sub-populations without relying on fitting the burst-based mean nanotime histograms to sums of Gaussians or other fitting functions (Fig. 4). We are then able to determine the mean photon nanotime of each state. For all labeled residues, these are centered at ~1.0 and ~2.2 ns. It is important to remember in that context that PIFE reports on dye-protein proximities within 0–3 nm (5,6), where 3 nm yields no fluorescence enhancement, hence low fluorescence lifetime values, and close to 0 nm yields the maximal fluorescence enhancement, hence highest fluorescence lifetime values. Additionally, in PIFE, the distance that is indirectly reported from changes in fluorescence lifetimes is between the sCy3 dye and protein parts that are in close proximity, which sterically obstruct the sCy3 *cis-trans* photoisomerization. Such effects at such proximities are well within what is considered as local interactions in proteins. Therefore, the ~1.0 ns sub-population represents an a-syn conformation with high degree of steric obstruction to the sCy3-labeled residues, and the ~2.2-ns sub-population represent a different a-syn conformation with lower degree of steric obstruction to the sCy3-labeled residue.

Thus, we demonstrate that mpH^{2}MM is capable of quantitatively characterizing transition dynamics in experimental data, such as smPIFE of the unbound a-syn monomer.

DISCUSSION

Using the divisor-based approach in mpH^{2}MM, we are able to reduce the intractably large and exponentially distributed parameter of fluorescence nanotimes into a tractable set of parameters, enabling the detection of within-burst lifetime state dynamics using mpH^{2}MM. This is especially powerful as both the fluorescence decays of states and transition rates are simultaneously recovered. This was applied in the case of smPIFE data, where the primary parameter is the mean fluorescence nanotime per state. Given a sufficiently bright sub-population, we are able to resolve transition rates and mean fluorescence lifetime values reliably.

Using mpH^{2}MM analysis, we recover the millisecond dynamics occurring between two major states in the unbound a-syn monomer. In these results, each state has a different mean fluorescence nanotime value that can, among other factors, represent different degrees of steric restriction imposed on the sCy3 dye conjugated to a specific residue in a-syn. This, in turn, reports on millisecond dynamics in structures that locally influence the vicinity of the dye-conjugated residue. We show that this millisecond local structural dynamics occurs within bursts in the vicinity of residues 56 in the edge region of the N-terminal segment of a-syn, and 140 at the terminus of the acidic C-terminal segment of a-syn. We could not recover within-burst lifetime-based dynamics in the vicinity of residue 26 in the N-terminal segment. However, the burst-based mean nanotime histograms report on multiple sub-populations, which points toward lifetime-based dynamics in the vicinity of this residue slower than burst durations. Combined with past results from smFRET-based measurements (38,45), we can propose that a-syn is a protein that exhibits intrinsic disorder characteristics between residues far apart along the primary sequence, perhaps representing

no stable nonlocal interactions, with millisecond stable local interactions that may promote stable local structural elements. Now, with the ability to identify and quantify within-burst dynamics in smPIFE measurements, and by doing so enhance the description of dynamics in biomolecules, we believe smPIFE could be used to study many other biomolecular systems.

While the divisor-based mpH^{2}MM approach has been shown here to uniquely aid in analyzing fluorescence lifetime-based within-burst dynamics, it is important to mention that the 2Dfluorescence lifetime correlation (2D-FLC) methodology (17,18,50) can help in such analyses. In 2D-FLC, inverse-Laplace transforms of 2D nanotime correlation functions produce 2D lifetime population maps. While the 2D-FLC is reported to be sensitive to within-burst dynamics as rapid as the typical microsecond interphoton times, the necessity of inverse-Laplace transformation of the data might require more photon data relative to the divisor-based mpH^{2}MM approach. Notably, our measurements typically lasted for 1–4 h, striving to achieve the best burst search and selection results with the best statistics. In contrast, when performing 2D-FLC, Ishii and Tahara performed data acquisition for a total of 25 h (18). In that context, it is noteworthy that our simulated datasets were attained from simulations of only 10 min, and that was still sufficient for retrieving the ground-truth parameters at a fair accuracy. Therefore, we assume that, while both approaches might be complementary in analyzing single dye fluorescence lifetime-based dynamics, the divisor-based mpH^{2}MM approach might fit the low number of photon nanotimes in each single-molecule burst for a lesser amount of bursts. Importantly, dynamics in the millisecond and sub-millisecond timescales many times do not provide a full picture of the fluorescence-based dynamics. In many ways, different modalities of fluorescence correlation spectroscopy (FCS) employed on freely-diffusing single molecules traversing through a confocal spot can also report on fluorescence-based dynamics in the microsecond timescale or even faster (see full coverage in a recent review (2)). However, these approaches might not solely report on transitions between different conformationally related states but also between bright fluorescent states and dark photo-blinked states, and it might be difficult to distinguish between these different processes solely based on FCS of single dye fluorescence data.

In this work, we tested the application of the divisor-based mpH^{2}MM approach for analyzing fluorescence lifetime-based single-molecule burst data assuming that the fluorescence lifetimes are linearly proportional to the fluorescence quantum yield (51), and also assuming fluorescence modulation is due solely to excited-state modulation (e.g., quenching or enhancement). However, ground-state modulation, such as ground-state quenching, could also exist in the data but not be represented by dynamics between fluorescence lifetime states. At the extreme case, such ground-state modulation that leads to fluorescence dynamics will be seen as dynamics between two states with different brightness values and no difference in fluorescence lifetime values. Therefore, to shed light on these additional possibilities, we suggest data treatments as were previously suggested by Kondo et al. (50), namely to present also the brightness in units of photons per millisecond of each dwell or burst, where a single molecule was identified as being in a given fluorescence lifetime state, in a 2D brightness versus lifetime map. In such a map, sub-populations off the diagonal represent a fraction of ground-state and excited-state modulation dynamics.

While the divisor-based approach to integrating photon nanotimes into mpH^{2}MM is typically applicable to PIFE, it is also possible to apply it to other modalities that include photon nanotimes, such as with single-molecule FRET. However, since FRET efficiencies and fluorescence lifetimes are intrinsically linked, barring additional complicated protein interactions, this also has the potential to introduce redundant data. Nevertheless, there are situations in which the ratiometric FRET efficiency parameter values differ from the FRET efficiency parameter values calculated from donor fluorescence lifetimes. One such case is when the doubly labeled system exhibits within-burst donoracceptor distance dynamics that can even be faster than the typical interphoton times. This deviation occurs due to the dynamics, where the high FRET state has not only lower donor lifetime than the lower FRET state but also less donor fluorescence photons, a situation analogous to the changes in both fluorescence lifetime and quantum yield in PIFE. Understanding the sources of these differences paved the way for Seidel and co-workers to develop an analytical framework dubbed FRET-Lines (52) to retrieve the underlying FRET dynamics from multi-parameter fluorescence detection (MFD) time-resolved smFRET measurements (53–55). In parallel to this approach, we provide the mpH^{2}MM approach for analyzing and quantifying within-burst dynamics in such confocal-based single-molecule measurements that refer to ratiometric FRET efficiency, donor and acceptor fluorescence lifetimes, fluorescence anisotropies, and other parameters. However, note that we currently do not gain any additional useful information from applying the MFD approach, compared with our previously implemented version of mpH^{2}MM, if neither the donor nor the acceptor are undergoing changes independent of FRET. Nevertheless, there are modalities, such as the combined PIFE-FRET (19), in which this analysis can be useful, to decouple three types of within-burst dynamics: 1) FRET dynamics, 2) PIFE dynamics, and 3) photophysical dynamics. In fact, retrieving the mean values from mpH^{2}MM analyses of PIFE-FRET could help in linking these values to their underlying physical meanings by using the existing theoretical framework of PIFE-FRET (8).

Incorporating more parameters combats the limited information content of single-molecule methods, which favor high time resolution, at the expense of spatial information. The more parameters are available in analysis, the greater is the ability to resolve and predict the unique properties of each conformational sub-population. The divisor approach removes one more limitation by allowing any parameter, including ones that do not centrally distribute, to be converted into a tractable ratiometric parameter that can then be used in data analyses such as mpH^{2}MM. This, in turn, brings us one step closer to a full picture of the microstates of biomolecules.

EXPERIMENTAL METHODS

smPIFE measurements of sCy3-labeled a-syn variants

The whole preparative procedure, from the expression, through the dye labeling, to the purification, were explained in full by Zaer and Lerner (20).

All smPIFE measurements and burst analyses of a-syn were performed and analyzed exactly as recently explained in Chen, Zaer et al. (46).

PyBroMo simulations

In PyBroMo, 20 particles in an $8 \times 8 \times 12$-μm^3 box are simulated with a diffusion constant of 12 μm^2/s. The time step of the simulation was set to 500 ns. Once single-molecule diffusion trajectories were built, then PyBroMo simulated the macrotime of photon detections. The point spread function (PSF) numerically solved and provided by PSFlab (56) is used to calculate the photon detection rate of each simulated single molecule at each moment, with different photon rates at the center of the PSF, better known as the molecular brightness values per each state. Then, the instantaneous photon rates are used for sampling detected photons out of the Poisson distribution with these photon rates. Then, background photons are added using a background count rate of 500 counts per second. Four different molecular brightness values were simulated for each molecule, one for each of the possible states, of which two will be selected once the final trajectory is built. Since molecular brightness and lifetime in fluorescence lifetime-based applications such as PIFE have been shown to linearly depend on each other, a universal base molecular brightness and base fluorescence lifetime are set as 275,000 counts per second, and 4.0 ns respectively. Then, ratios of 0.3, 0.4, 0.8, and 0.9 are set as degrees of effects on reducing the molecular brightness and the fluorescence lifetime. Multiplying the base value by the ratio leads to the actual value used in each simulation. For the simulation of states with multi-exponential fluorescence decays, an additional decay with a base lifetime of 1.2 ns is incorporated. This shorter lifetime component is also scaled with the ratio of the brightness and lifetime reduction effect. This shorter lifetime component contributes 10% of the photons in the simulations of states with multi-exponential fluorescence decays.

PyBroMo simulates photon detection times. However, it does not yet simulate either photon nanotimes or dynamic transitions between lifetime-based states. Therefore, these effects were added through additional layers after PyBroMo simulations. To simulate photon nanotimes, a Monte-Carlo simulation is used, simulating an exponential fluorescence decay, and then adding an additional delay pulled from the experimental IRF of our setup, described in Zaer and Lerner (20). Drawing on previous work, transitions between states are made by stitching photon trajectories together. First, dwell times in each state are simulated by taking random exponential distributions based on the transition rate. This forms time windows for each molecule when it is in a given state. Then, for each simulated state, photons within those time windows are selected, and stitched together to create the final photon trajectories of simulations.

Burst search and selection

Both simulated and experimental data are imported into FRETBursts (31), and background is first assessed for each time interval of 30 s. Then, burst search is performed by selecting bursts with an instantaneous count rate of F = 6 times the background rate, with the instantaneous count rate calculated using a sliding window of m = 10 photons. Bursts are further refined to require a minimum width of 1 ms, a minimum peak count rate of 20,000 counts per second, and a minimum size of 25 photons.

This provided the base burst selection on which all downstream processing was conducted. Whenever mean nanotimes are discussed, a threshold is set denoting the end of the IRF.

The mean delay of photons arriving after this threshold relative to said threshold is then calculated, and this is the mean nanotime. Photons arriving before this threshold are excluded from the mean nanotime analysis. This method is applied equally to burst- and dwell-based mean nanotimes and used in BVA calculations.

mpH^{2}MM analysis

In mpH^{2}MM, photons must be assigned indices, which are assigned based on the bin into which the photon nanotime is collected. We test a total of eight different divisor schemes that assign photons to bins differently. These divisor schemes differ in how many divisors are used, and whether or not the IRF was assigned to its own bin. Thus, divisor schemes can be assigned into two groups: the non-IRF and with IRF divisor schemes. For non-IRF scheme, the divisors were set to equally divide the total photon nanotimes of all photons within bursts into bins. Thus, if there was one divisor, it would be placed at the 50th percentile; if two divisors, at the 33rd and 66th percentiles. The IRF schemes followed a similar pattern, except that an additional divisor was set at the end of the IRF, and the percentiles were assigned according to the nanotimes of only photons that arrived after the IRF divisor. We test from one to four divisors in the non-IRF scheme, and one to four divisors (which have n + 1 divisors due to the additional divisor of the IRF) in the IRF scheme. All analyses were performed using the H2MM_C python package (22). Model optimizations were performed on single-, two-, and three-state models. The Viterbi algorithm was then applied to determine the most-likely state path-based optimized model, and to determine the ICL of each optimization. The state path was then segmented into state dwells, on which duration and mean photon nanotimes could be assessed. Further, using the most-likely state assignment, the photon nanotimes are assembled to create state-based fluorescent decays. Finally, for analysis of the accuracy of the state assignment, the state assigned by Viterbi is compared with the ground-truth of the simulation. For this comparison, photons are assigned as correct, incorrect, or not applicable, when the ground-truth origin of the photon was either background or from a molecule that did not contribute the majority of photons in the burst. In this final case, the result of applying the Viterbi algorithm is ignored. For the assessment of the fraction of photons correctly assigned to a state, these background photons are excluded. For mpH^{2}MM analysis of a-syn data, optimizations are carried out for increasing numbers of states until the ICL ceases to decrease.

Supporting Material

Supporting Material contains additional details on methods for (i) calculating BVA and 2CDE, (ii) figures mirroring Figs. 2 and 3 for other combinations of long and short lifetime states, and for truncated simulations, (iii) figures detailing over-fit models, (iv) recovered transition rates compared with the ground truth, (v) a table of the number of states in the ICL selected model for all simulations.

Data availability

All the code, simulations, experimental and simulated data files, and the data analyses in Jupyter Notebooks are available publicly over Zenodo, in the following hyperlink: https://doi.org/10.5281/zenodo.6591249.

Supplementary Material

Refer to Web version on PubMed Central for supplementary material.

ACKNOWLEDGMENTS

APPENDIX

In general, fluorescence quantum yield and fluorescence intensity are linearly proportional to the fluorescence lifetime. In PIFE, the primary modulator of both fluorescence intensity and lifetime is via the competition between emission from a bright excited-state isomer and the photo-isomerization into dark states. Thus, we can derive the relationship through Eq. 2 (51):

$$\varphi_f = \frac{k_f}{k_f + k_{ic} + k_{Nt}} = k_f\tau \tag{2}$$

where φ_f is the fluorescence quantum yield, k_f is the radiative rate due to fluorescence, k_{ic} is the nonradiative rate due to internal conversion, k_{Nt} is the rate of de-excitation through excited-state isomerization, and τ is the observed fluorescence lifetime. Thus φ_f and τ are directly and linearly proportional.

REFERENCES

1. Ha T, Enderle T, …, Weiss S. 1996. Probing the Interaction between Two Single Molecules: Fluorescence Resonance Energy Transfer between a Single Donor and a Single Acceptor. Proc. Natl. Acad. Sci. USA. 93:6264–6268. 10.1073/pnas.93.13.6264. [PubMed: 8692803]

2. Lerner E, Cordes T, …, Weiss S. 2018. Toward Dynamic Structural Biology: Two Decades of Single-Molecule Förster Resonance Energy Transfer. Science. 359:eaan1133. 10.1126/science.aan1133. [PubMed: 29348210]

3. Haenni D, Zosel F, …, Schuler B. 2013. Intramolecular Distances and Dynamics from the Combined Photon Statistics of Single-Molecule FRET and Photoinduced Electron Transfer. J. Phys. Chem. B. 117:13015–13028. 10.1021/jp402352s. [PubMed: 23718771]

4. Pantazis A, Westerberg K, …, Olcese R. 2018. Harnessing Photoinduced Electron Transfer to Optically Determine Protein Sub-Nanoscale Atomic Distances. Nat. Commun. 9:4738. 10.1038/s41467-018-07218-6. [PubMed: 30413716]

5. Hwang H, Kim H, and Myong S. 2011. Protein Induced Fluorescence Enhancement as a Single Molecule Assay with Short Distance Sensitivity. Proc. Natl. Acad. Sci. USA. 108:7414–7418. 10.1073/pnas.1017672108. [PubMed: 21502529]

6. Hwang H, and Myong S. 2014. Protein Induced Fluorescence Enhancement (PIFE) for Probing Protein-Nucleic Acid Interactions. Chem. Soc. Rev. 43:1221–1229. 10.1039/c3cs60201j. [PubMed: 24056732]

7. Stennett EMS, Ciuba MA, …, Demystifying PIFE. 2015. The photophysics behind the protein-induced fluorescence enhancement phenomenon in Cy3. J. Phys. Chem. Lett 6:1819–1823. 10.1021/acs.jpclett.5b00613. [PubMed: 26263254]

8. Lerner E, Ploetz E, …, Weiss S. 2016. A Quantitative Theoretical Framework For Protein-Induced Fluorescence Enhancement–Förster-Type Resonance Energy Transfer (PIFE-FRET). J. Phys. Chem. B. 120:6401–6410. 10.1021/acs.jpcb.6b03692. [PubMed: 27184889]

9. Steffen FD, Sigel RKO, and Börner R. 2016. An Atomistic View on Carbocyanine Photophysics in the Realm of RNA. Phys. Chem. Chem. Phys. 18:29045–29055. 10.1039/C6CP04277E. [PubMed: 27783069]

10. Kim H, Lee CY, …, Park HG. 2018. Protein-induced fluorescence enhancement for a simple and universal detection of protein/small molecule interactions. RSC Adv. 8:39913–39917. 10.1039/C8RA08515C. [PubMed: 35558217]

11. Dahan M, Deniz AA, …, Weiss S. 1999. Ratiometric Measurement and Identification of Single Diffusing Molecules. Chem. Phys. 247:85–106. 10.1016/S0301-0104(99)00132-9.

12. Deniz AA, Dahan M, …, Schultz PG. 1999. Single-Pair Fluorescence Resonance Energy Transfer on Freely Diffusing Molecules: Observation of Forster Distance Dependence and Subpopulations. Proc. Natl. Acad. Sci. USA. 96:3670–3675. 10.1073/pnas.96.7.3670. [PubMed: 10097095]

13. Gopich IV, and Szabo A. 2006. Theory of the Statistics of Kinetic Transitions with Application to Single-Molecule Enzyme Catalysis. J. Chem. Phys. 124:154712. 10.1063/1.2180770. [PubMed: 16674256]

14. Torella JP, Holden SJ, …, Kapanidis AN. 2011. Identifying Molecular Dynamics in Single-Molecule Fret Experiments with Burst Variance Analysis. Biophys. J. 100:1568–1577. 10.1016/j.bpj.2011.01.066. [PubMed: 21402040]

15. Lerner E, Ingargiola A, and Weiss S. 2018. Characterizing Highly Dynamic Conformational States: The Transcription Bubble in RNAP-Promoter Open Complex as an Example. J. Chem. Phys. 148:123315. 10.1063/1.5004606. [PubMed: 29604842]

16. Haustein E, and Schwille P. 2007. Fluorescence Correlation Spectroscopy: Novel Variations of an Established Technique. Annu. Rev. Biophys. Biomol. Struct. 36:151–169. 10.1146/annurev.biophys.36.040306.132612. [PubMed: 17477838]

17. Ishii K, and Tahara T. 2013. Two-Dimensional Fluorescence Lifetime Correlation Spectroscopy. 1. Principle. J. Phys. Chem. B. 117:11414–11422. 10.1021/jp406861u. [PubMed: 23977832]

18. Ishii K, and Tahara T. 2013. Two-Dimensional Fluorescence Lifetime Correlation Spectroscopy. 2. Application. J. Phys. Chem. B. 117:11423–11432. 10.1021/jp406864e. [PubMed: 23977902]

19. Ploetz E, Lerner E, …, Cordes T. 2016. Förster Resonance Energy Transfer and Protein-Induced Fluorescence Enhancement as Synergetic Multi-Scale Molecular Rulers. Sci. Rep. 6 (ptember):33257–33318. 10.1038/srep33257. [PubMed: 27641327]

20. Zaer S, and Lerner E. 2021. Utilizing time-resolved protein-induced fluorescence enhancement to identify stable local conformations one α-synuclein monomer at a time. J. Vis. Exp. 171:e62655. 10.3791/62655.

21. Pirchi M, Tsukanov R, …, Nir E. 2016. Photon-by-photon hidden markov model analysis for microsecond single-molecule fret kinetics. J. Phys. Chem. B. 120:13065–13075. 10.1021/acs.jpcb.6b10726. [PubMed: 27977207]

22. Harris PD, Narducci A, …, Lerner E. 2022. Multi-Parameter Photon-by-Photon Hidden Markov Modeling. Nat. Commun. 13:1000–1012. 10.1038/s41467-022-28632-x. [PubMed: 35194038]

23. Sisamakis E, Valeri A, …, Seidel CAM. 2010. Accurate Single-Molecule FRET Studies Using Multiparameter Fluorescence Detection. In Methods in Enzymology, 475. Elsevier Inc., pp. 455–514. 10.1016/S0076-6879(10)75018-7. [PubMed: 20627168]

24. Digman MA, Caiolfa VR, …, Gratton E. 2008. The Phasor Approach to Fluorescence Lifetime Imaging Analysis. Biophys. J. 94:L14–L16. 10.1529/biophysj.107.120154. [PubMed: 17981902]

25. Kapanidis AN, Laurence TA, …, Weiss S. 2005. Alternating-Laser Excitation of Single Molecules. Acc. Chem. Res. 38:523–533. 10.1021/ar0401348. [PubMed: 16028886]

26. Lee NK, Kapanidis AN, …, Weiss S. 2005. Accurate FRET measurements within single diffusing biomolecules using alternating-laser excitation. Biophys. J. 88:2939–2953. 10.1529/biophysj.104.054114. [PubMed: 15653725]

27. Laurence TA, Kong X, …, Weiss S. 2005. Probing Structural Heterogeneities and Fluctuations of Nucleic Acids and Denatured Proteins. Proc. Natl. Acad. Sci. USA. 102:17348–17353. 10.1073/pnas.0508584102. [PubMed: 16287971]

28. Muller BK, Zaychikov E, …, Lamb DC. 2005. Pulsed Interleaved Excitation. Biophys. J. 89:3508–3522. 10.1529/biophysj.105.064766. [PubMed: 16113120]

29. Ingargiola A OpenSMFS/PyBroMo: Version 0.8.1. 10.5281/zenodo.3256149.

30. Hagai D, and Lerner E. 2019. Systematic Assessment of Burst Impurity in Confocal-Based Single-Molecule Fluorescence Detection Using Brownian Motion Simulations. Molecules. 24:E2557. 10.3390/molecules24142557. [PubMed: 31337081]

31. Ingargiola A, Lerner E, …, Michalet X. 2016. FRETBursts: An Open Source Toolkit for Analysis of Freely-Diffusing Single-Molecule FRET. PLoS One. 11. e0160716–27. 10.1371/journal.pone.0160716. [PubMed: 27532626]

32. Tomov TE, Tsukanov R, …, Nir E. 2012. Disentangling Subpopulations in Single-Molecule FRET and ALEX Experiments with Photon Distribution Analysis. Biophys. J. 102:1163–1173. 10.1016/j.bpj.2011.11.4025. [PubMed: 22404939]

33. Goedert M 2001. Alpha-Synuclein and Neurodegenerative Diseases. Nat. Rev. Neurosci. 2:492–501. 10.1038/35081564. [PubMed: 11433374]

34. Kayed R, Dettmer U, and Lesné SE. 2020. Soluble Endogenous Oligomeric α-Synuclein Species in Neurodegenerative Diseases: Expression, Spreading, and Cross-Talk. J. Parkinsons Dis. 10:791–818. 10.3233/JPD-201965. [PubMed: 32508330]

35. Gómez-Benito M, Granado N, …, Moratalla R. 2020. Modeling Parkinson's Disease With the Alpha-Synuclein Protein. Front. Pharmacol. 11:356. [PubMed: 32390826]

36. Ulmer TS, Bax A, …, Nussbaum RL. 2005. Structure and Dynamics of Micelle-Bound Human α-Synuclein. J. Biol. Chem. 280:9595–9603. 10.1074/jbc.M411805200. [PubMed: 15615727]

37. Georgieva ER, Ramlall TF, …, Eliezer D. 2008. Membrane-Bound α-Synuclein Forms an Extended Helix: Long-Distance Pulsed ESR Measurements Using Vesicles, Bicelles, and Rodlike Micelles. J. Am. Chem. Soc. 130:12856–12857. 10.1021/ja804517m. [PubMed: 18774805]

38. Ferreon ACM, Gambin Y, …, Deniz AA. 2009. Interplay of α-Synuclein Binding and Conformational Switching Probed by Single-Molecule Fluorescence. Proc. Natl. Acad. Sci. USA. 106:5645–5650. 10.1073/pnas.0809232106. [PubMed: 19293380]

39. Bartels T, Choi JG, and Selkoe DJ. 2011. α-Synuclein Occurs Physiologically as a Helically Folded Tetramer That Resists Aggregation. Nature. 477:107–110. 10.1038/nature10324. [PubMed: 21841800]

40. Wang W, Perovic I, …, Hoang QQ. 2011. A Soluble α-Synuclein Construct Forms a Dynamic Tetramer. Proc. Natl. Acad. Sci. USA. 108:17797–17802. 10.1073/pnas.1113260108. [PubMed: 22006323]

41. Celej MS, Sarroukh R, …, Raussens V. 2012. Toxic Prefibrillar α-Synuclein Amyloid Oligomers Adopt a Distinctive Antiparallel β-Sheet Structure. Biochem. J. 443:719–726. 10.1042/BJ20111924. [PubMed: 22316405]

42. Alam P, Bousset L, …, Otzen DE. 2019. α-Synuclein Oligomers and Fibrils: A Spectrum of Species, a Spectrum of Toxicities. J. Neurochem. 150:522–534. 10.1111/jnc.14808. [PubMed: 31254394]

43. Zhou L, and Kurouski D. 2020. Structural Characterization of Individual α-Synuclein Oligomers Formed at Different Stages of Protein Aggregation by Atomic Force Microscopy-Infrared Spectroscopy. Anal. Chem. 92:6806–6810. 10.1021/acs.analchem.0c00593. [PubMed: 32347706]

44. Theillet F-X, Binolfi A, …, P. Selenko. 2016. Structural Disorder of Monomeric α-Synuclein Persists in Mammalian Cells. Nature. 530:45–50. 10.1038/nature16531. [PubMed: 26808899]

45. Rezaei-Ghaleh N, Parigi G, …, Zweckstetter M. 2018. Local and Global Dynamics in Intrinsically Disordered Synuclein. Angew. Chem., Int. Ed. Engl. 57:15262–15266. 10.1002/anie.201808172. [PubMed: 30184304]

46. Chen J, Zaer S, …, Dokholyan NV. 2021. The Structural Heterogeneity of α-Synuclein Is Governed by Several Distinct Subpopulations with Interconversion Times Slower than Milliseconds. Structure. 29:1048–1064.e6. 10.1016/j.str.2021.05.002. [PubMed: 34015255]

47. Luitz MP, Barth A, …, Zacharias M. 2017. Covalent Dye Attachment Influences the Dynamics and Conformational Properties of Flexible Peptides. PLoS One. 12. . e0177139–18. 10.1371/journal.pone.0177139. [PubMed: 28542243]

48. Van den Berg PAW, Feenstra KA, …, Visser AJWG. 2002. Dynamic Conformations of Flavin Adenine Dinucleotide: Simulated Molecular Dynamics of the Flavin Cofactor Related to the Time-Resolved Fluorescence Characteristics. J. Phys. Chem. B. 106:8858–8869. 10.1021/jp020356s.

49. Hoffmann A, Nettels D, …, Schuler B. 2011. Quantifying Heterogeneity and Conformational Dynamics from Single Molecule FRET of Diffusing Molecules: Recurrence Analysis of Single Particles (RASP). Phys. Chem. Chem. Phys. 13:1857–1871. 10.1039/c0cp01911a. [PubMed: 21218223]

50. Kondo T, Pinnola A, …, Schlau-Cohen GS. 2017. Single-Molecule Spectroscopy of LHCSR1 Protein Dynamics Identifies Two Distinct States Responsible for Multi-Timescale Photosynthetic Photoprotection. Nat. Chem. 9:772–778. 10.1038/nchem.2818. [PubMed: 28754946]

51. Sanborn ME, Connolly BK, …, Levitus M. 2007. Fluorescence Properties and Photophysics of the Sulfoindocyanine Cy3 Linked Covalently to DNA. J. Phys. Chem. B. 111:11064–11074. 10.1021/jp072912u. [PubMed: 17718469]

52. Barth A, Opanasyuk O, …, Seidel CAM. 2022. Unraveling Multi-State Molecular Dynamics in Single-Molecule FRET Experiments- Part I: Theory of FRET-Lines. J. Chem. Phys. 156:141501. 10.1063/5.0089134. [PubMed: 35428384]

53. Rothwell PJ, Berger S, …, Seidel CAM. 2003. Multiparameter Single-Molecule Fluorescence Spectroscopy Reveals Heterogeneity of HIV-1 Reverse Transcriptase:Primer/Template Complexes. Proc. Natl. Acad. Sci. USA. 100:1655–1660. 10.1073/pnas.0434003100. [PubMed: 12578980]

54. Widengren J, Kudryavtsev V, …, Seidel CAM. 2006. Single-Molecule Detection and Identification of Multiple Species by Multiparameter Fluorescence Detection. Anal. Chem. 78:2039–2050. 10.1021/ac0522759. [PubMed: 16536444]

55. Kalinin S, Felekyan S, …, Seidel CAM. 2008. Characterizing Multiple Molecular States in Single-Molecule Multiparameter Fluorescence Detection by Probability Distribution Analysis. J. Phys. Chem. B. 112:8361–8374. 10.1021/jp711942q. [PubMed: 18570393]

56. Nasse MJ, and Woehl JC. 2010. Realistic Modeling of the Illumination Point Spread Function in Confocal Scanning Optical Microscopy. J. Opt. Soc. Am. Opt Image Sci. Vis 27:295–302. 10.1364/JOSAA.27.000295.

WHY IT MATTERS

Single dye-based single-molecule spectroscopic experiments, which rely on fluorescence lifetime, simplify sample preparation. However, methods for data analysis have lagged behind those of their two dye Förster resonance energy transfer (FRET)-based counterparts. Particularly, while methods to detect sub-millisecond dynamics existed for single-molecule FRET, for their single dye lifetime-based counterparts, they were lacking. Products of this work enable detection and quantification of sub-millisecond within-burst dynamics in lifetime-based single-molecule fluorescence spectroscopy measurements. Using the presented divisor-based approach, we demonstrate the ability to quantify lifetime-based states, their mean fluorescence lifetimes, and their transition rates for dynamically interconverting singly labeled biomolecules. We then show the usefulness of the method on retrieving millisecond dynamics in single-molecule photo-isomerization-related fluorescence enhancement (smPIFE) measurements, which was difficult to achieve before.
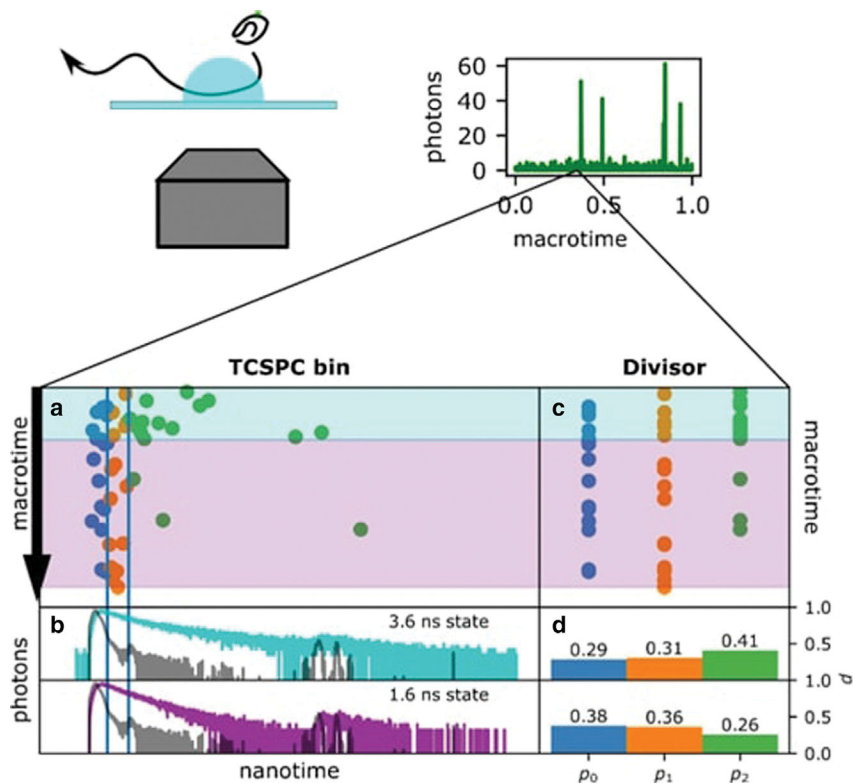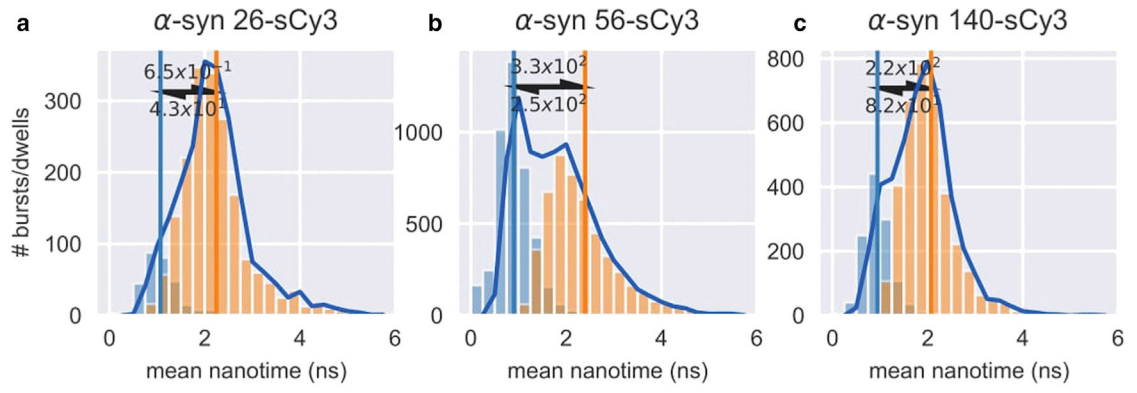
FIGURE 1.

The divisor-based approach to analyzing within-burst fluorescence lifetime dynamics. (*a*) Simulated burst of photons originating from a molecule dye labeled with sCy3, which undergoes fluorescence lifetime transition while traversing the laser focus. The absolute detection times of photons (i.e., the photon macrotimes) are represented on the vertical axis, and the photon nanotimes on the horizontal axis. The vertical lines indicate divisors separating photon nanotimes into bins. (*b*) The simulated decays of the states are given in colored lines. The IRF is given in grey lines. (*c*) The same burst but with photons organized by bins, not nanotimes. (*d*) The probability of a photon arriving in each divisor for the two states.
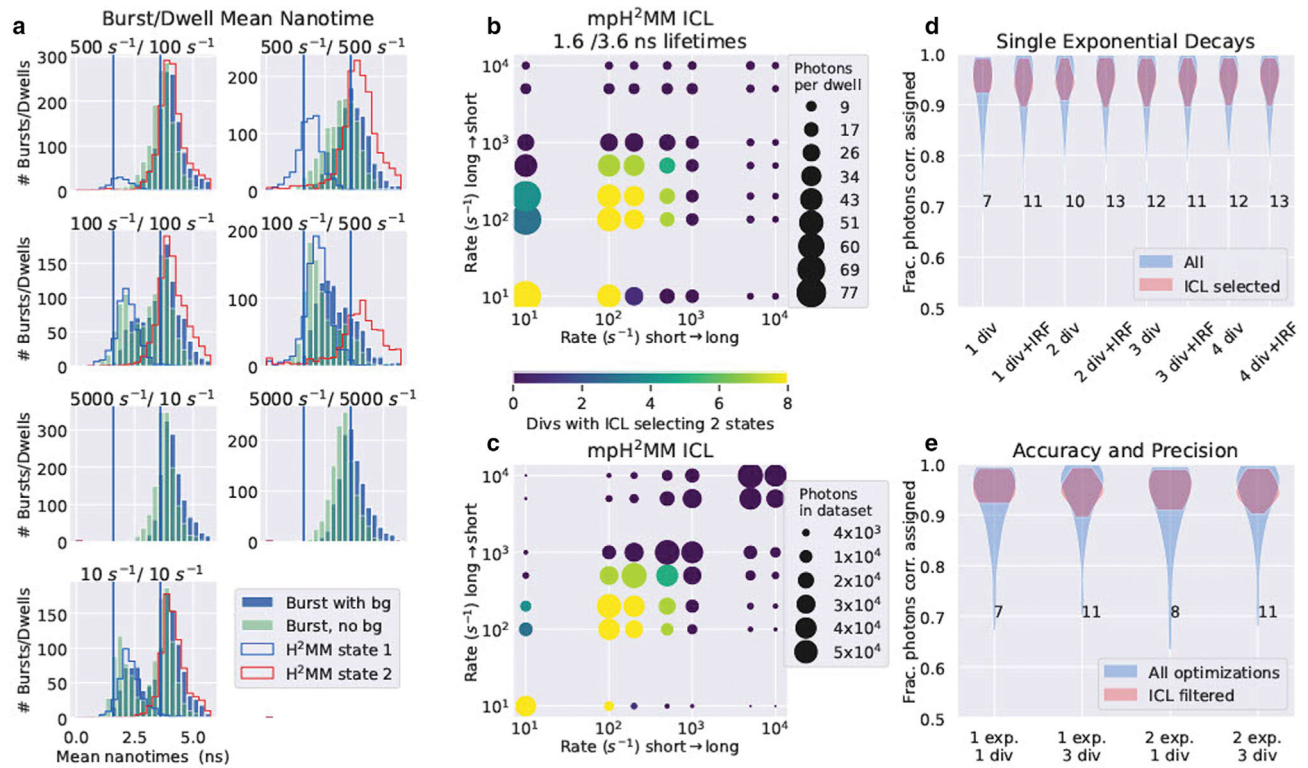
FIGURE 2.

Sensitivity of mpH²MM in divisor-based fluorescence lifetime analysis. (*a*) Selected examples of mean nanotime histograms of simulated data. Vertical bars indicate the ground-truth lifetime values. Filled-bar histograms are mean nanotimes of bursts, blue of data including simulated background, while teal bars are the same data but with background photons excluded from calculation of mean nanotimes. Stepped-line histograms show mean nanotimes of dwells in a state within a burst determined by mpH²MM analysis. (*b* and *c*) The minimization of the statistic, ICL, and its capability to correctly identify the number of states. Color indicates the number of divisor schemes where the ICL was minimized for the ground-truth two-state models. In (*b*), the size of the spot indicates the mean number of photons in a dwell within a burst, for the state with the least number of photons per dwell. In (*c*), the size of the spot indicates, for the less populated state, how many photons from that state were available across all bursts. (*d* and *e*) Violin plots of the fraction of photons whose most-likely state from mpH²MM analysis determined by the Viterbi algorithm matched that of the state known by the ground truth. In (*d*), different divisor schemes for simulations using single exponential decays are compared. In (*e*), different divisors and simulations with mono- and bi-exponential decays are compared. Numbers indicate the number of mpH²MM models of the given divisor/decay combination whose ICL was minimized for the ground-truth two-state model.
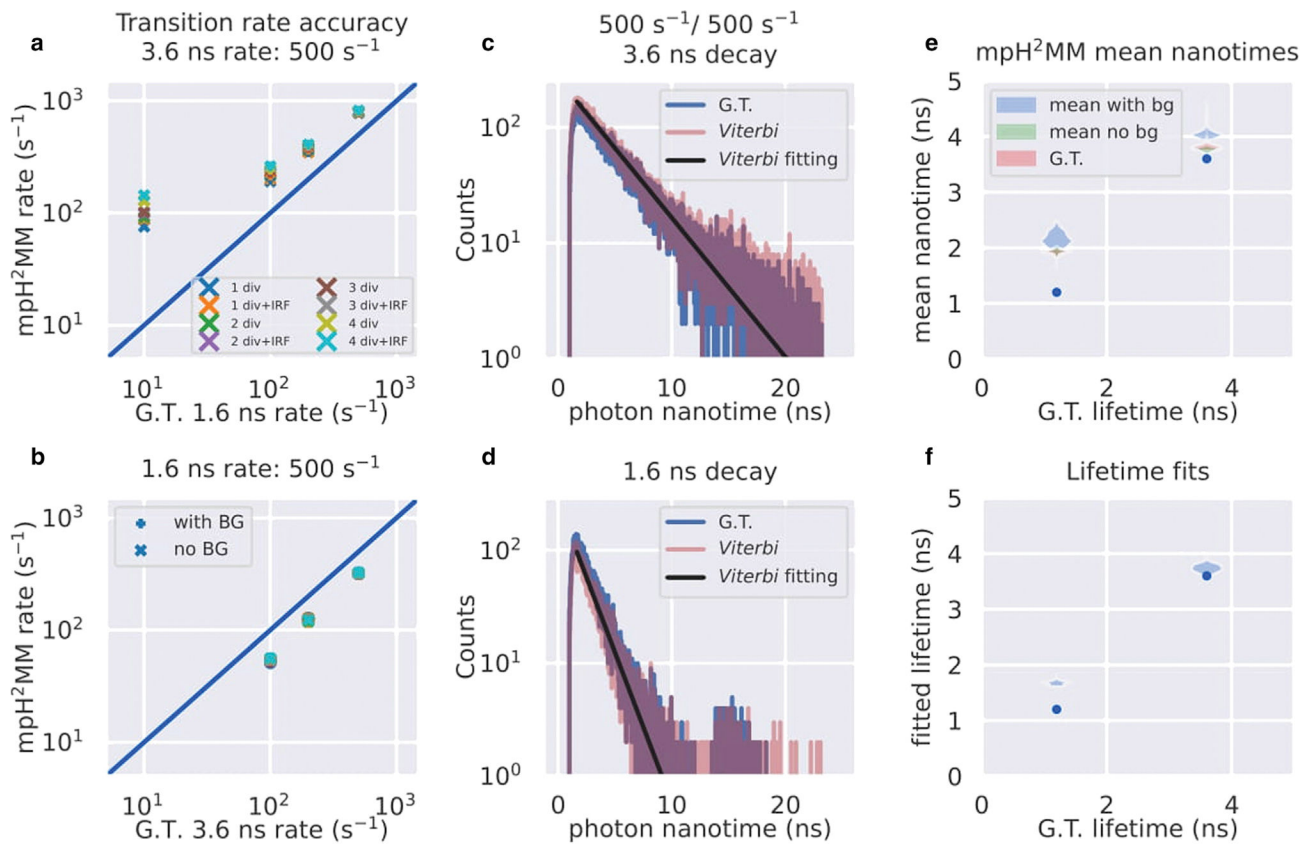
FIGURE 3.

Assessment of mpH²MM in determining transition rates and lifetimes. (*a* and *b*) The ground-truth transition rate versus mpH²MM. Horizontal axis compares transition rate from the (*a*) 3.6 ns or (*b*) 1.6 ns states. In all panels, the transition rate from the other state is held constant at 500 s⁻¹. Plus signs (+) indicate mpH²MM optimizations with all photons, while × signs indicate optimizations where background photons were excluded. (*c* and *d*) Comparison of fluorescence decays of the ground-truth (blue) and reconstructed based on most-likely state derived from the Viterbi algorithm employed on the results of mpH²MM analyses of the simulated data (*red*). Black line shows bi-exponential fitting of Viterbi-based fluorescence decay. Both are for simulations with 500 s⁻¹ transition rate for both states (i.e., the transition rates are symmetric); (*c*) 3.6 ns state, (*d*) 1.6 ns state. (*e*) Violin plot showing the mean nanotimes of all states using mpH²MM for all ICL selected models of simulations with states of 1.6 and 3.6 ns. Blue plots for data with background photons included, green for data with background photons excluded, and red of mean nanotimes derived from the ground-truth. (*f*) Violin plots of mono-exponential fittings of Viterbi-derived fluorescence decays of same data as in *e*). G.T., ground-truth.

FIGURE 4.

mpH^{2}MM analysis of the unbound α-syn monomer labeled at residues (*a*) 26, (*b*) 56, and (*c*) 140 with sCy3. Barred histograms indicate mean nanotimes of state dwells within bursts, while lined histograms indicate burst-based mean nanotimes.